RSC Advances

PAPER

View Article Online
View Journal | View Issue

Check for updates

Cite this: RSC Adv., 2025, 15, 25067

Atomic scale study for the structural evolution of monolayer 1T′-MoS_2†

Lei Xu,*[ab] Feng Li[c] and Junjie Qi *[a]

Received 11th April 2025
Accepted 7th July 2025

DOI: 10.1039/d5ra02532j

rsc.li/rsc-advances

Two-dimensional transition metal dichalcogenides (2D-TMDs) exhibit diverse polymorphic configurations characterized by distinct atomic arrangements and electronic properties. Harnessing phase transitions in TMDs can overcome spatial and technical limitations of conventional semiconductor fabrication, driving advancements in next-generation optoelectronics and energy conversion technologies. Herein, by performing *in situ* atomic-resolution characterization employing aberration-corrected scanning transmission electron microscopy (AC-STEM), the dynamic structural evolution in monolayer 1T′-MoS_2 were directly observed. Our observations demonstrate that the dynamic recombination of molybdenum–molybdenum bonds within the characteristic zigzag chains facilitates the formation of tetrameric metal clusters and subsequently induces a newly oriented zigzag chains of molybdenum, ultimately establishing anisotropic configurations. Notably, the 2H/1T′ grain boundaries maintain atomically sharp and coherent interfaces devoid of detectable lattice strain-a critical feature for constructing high-performance heterostructure devices requiring precise interfacial charge transport. These atomic-scale insights into structural evolution mechanisms not only advance fundamental understanding of phase transformation dynamics in 2D materials, but also provide crucial design principles for engineering metastable-phase architectures in functional nanoelectronics.

Introduction

Atomically thin TMDs have emerged as a unique class of materials due to their novel physical and chemical properties, demonstrating significant potential in electronic devices,[1–3] optical systems,[4,5] and catalytic applications.[6,7] A defining feature of layered TMDs is their polymorphism,[8] which enables precise structure–property engineering and has spurred extensive research into phase-dependent functionalities. The coordination geometry of TMDs is intrinsically linked to the electron population in the valence d-orbitals of their constituent transition metals.[9] For instance: Group IVB (d^0) and VIII (d^6) TMDs adopt octahedral coordination (1T phase), Group VB (d^1) systems exhibit mixed prismatic and octahedral configurations, Most Group VIB (d^2) TMDs stabilize in trigonal prismatic coordination (2H phase), Group VIIB (d^3) compounds predominantly form distorted octahedral structures (1T′ phase).[9,10] A representative case is MoS_2, which exists in metastable 1T and thermodynamically stable 2H phases. The 1H–MoS_2 phase exhibits semiconducting behavior with a bandgap arising from energy separation between filled d_{z^2} and empty $d_{x^2-y^2,\,xy}$ orbitals, while the metallic 1T phase features a Fermi level intersecting degenerate $d_{xy,\,yz,\,xz}$ bands.[11] The intrinsic properties of these phases are not merely academic curiosities but govern MoS_2's functionality across diverse applications. The thermodynamically stable 2H phase,[12] characterized by its trigonal prismatic coordination, possesses a direct bandgap in monolayer form, making it indispensable for next-generation electronics,[2,3] photodetectors,[4,5] valleytronics,[13,14] and catalytic processes[6,7] like hydrogen evolution. In stark contrast, the metastable 1T phase (often stabilized as the distorted 1T′ variant) adopts an octahedral coordination,[12] exhibiting metallic conductivity, enhanced hydrophilicity, and dramatically improved catalytic activity[12]—particularly for the hydrogen evolution reaction (HER)—owing to its favorable electronic structure and basal plane activation. There is a large energy difference[15] between 2H and 1T indicates that the 1T-MoS_2 is the most unstable and has a high distortion tendency. Consequently, similar to the Peierls distortion, the 1T phase will relax and buckle spontaneously into a thermodynamically more stable distorted structure known as the 1T′ phase, the structural distortion results in the removal of the degeneracy of the nested Fermi surface, and a 50–570 meV gap may be opened up in the electronic energy band structure.[15–17] The phase-dependent properties of MoS_2 underpin its versatility in both fundamental studies and technological applications. The

[a]School of Materials Science and Engineering, University of Science and Technology Beijing, Beijing 100083, P. R. China
[b]School of Materials Science and Engineering, Tsinghua University, Beijing 100084, P. R. China
[c]School of Biomedical Engineering, Shenzhen University Medical School, Shenzhen University, Shenzhen 518060, P. R. China. E-mail: junjieqi@ustb.edu.cn

† Electronic supplementary information (ESI) available. See DOI: https://doi.org/10.1039/d5ra02532j

semiconducting 2H phase is ideal for electronic/optoelectronic devices,[1,4,5] whereas the semi-metallic 1T/1T′ phases show promise in superconductivity research.[18] The profound divergence in electronic, optical, and chemical properties between these phases, arising solely from differences in atomic coordination within the same chemical composition, underscores the critical importance of phase engineering in MoS_2 research. Understanding and controlling the 2H-to-1T phase transition, or stabilizing hybrid heterophase structures, unlocks unprecedented opportunities to tailor material performance for specific applications.

In contrast to the extensively investigated 2H–MoS_2, the 1T′-MoS_2 phase has historically received limited research attention. Recent theoretical advances, however, have revealed its exceptional multi-configurational potential, including predictions of topological states such as Weyl semimetals[19,20] and quantum spin Hall effects,[17] as well as correlated phenomena like charge density waves (CDW)[21] and dipolar ferroelectricity.[22] Notably, 1T′-MoS_2 plays a pivotal role in enabling low-resistance contact engineering for 2D TMDs-based transistors.[23–25] Theoretical studies reveal that below the critical Peierls temperature (Tp), the elastic energy loss for atomic rearrangement during the 1T-to-1T′ structural transition in MoS_2 is less than the gain of electron energy. This thermodynamic preference triggers spontaneous periodic lattice distortions, which in turn induce electronic state condensation into a collective quantum ground state. The synergistic electron-lattice coupling generates coherent charge density modulations, ultimately stabilizing a CDW phase with characteristic (2×1) superlattice.[26] Phase engineering from H to T/T′ phase in MoS_2 can be achieved *via* multiple pathways, including alkali metal intercalation,[27] thermal activation,[28] and strain engineering[29,30] *etc.* 1T′-MoS_2 has emerged as an exceptional electrocatalyst for hydrogen evolution.[31–34] Additionally, it serves as an effective carrier injection contact for 2D field-effect transistors. The synergistic combination of these attributes situates 1T′-MoS_2 as a material with considerable potential for both fundamental physics research and advanced quantum devices applications.

Despite recent advancements have revitalized interest in technological applications of 1T′-MoS_2 materials, fundamental understanding of their structural configuration and stability remains incomplete. Atomic-resolution STEM, complemented by high-angle annular dark field (HAADF) imaging, emerges as an indispensable platform for atomic-scale characterization of 2D materials, enabling precise identification of monolayer configurations and edge structures with exceptional spatial resolution.[35,36] Our investigations reveal that electron beam irradiation induces dynamic structural reorganization in monolayer 1T′-MoS_2, manifested through bond reconfiguration in the characteristic zigzag molybdenum chains. This phenomenon leads to the emergence of newly crystalline orientations, demonstrating that controlled electron beam exposure can effectively modulate metal–metal bond order and induce anisotropic orientation preferences. Furthermore, atomic-scale characterization uncovers interfacial structures between distinct phases (2H/1T′), providing unprecedented insights into phase boundary configurations. The experimental methodology integrates *in situ* STEM to capture real-time structural evolution dynamics at atomic resolution. These observations offering new perspectives on phase transition mechanisms. The findings significantly advance our understanding of TMDs, particularly regarding phase-dependent electronic properties. This work establishes critical structure–property relationships that inform phase engineering strategies, potentially revolutionizing the design of next-generation electronic devices through precise control of quantum material phases.

Experimental section

Sample preparation

The chemically exfoliated MoS_2 (ce-MoS_2) was prepared as followed: In an argon-filled glovebox, 0.5 g of MoS_2 powder (Alfa Aesar, 99.8% purity) was thoroughly mixed with 0.1 g $LiBH_4$ (Merck, 99.5%) and subsequently annealed at 280 °C for 72 hours on a temperature-controlled hotplate to facilitate lithium ion intercalation. Following thermal treatment, the intercalated composite was transferred to deionized water for ultrasonic exfoliation (1 h at 40 kHz). To ensure complete removal of residual lithium ions, the resulting suspension underwent multiple centrifugation cycles (10 000 rpm, 1 h per cycle, minimum 5 repetitions), followed by vacuum filtration through a 0.45 μm PTFE membrane. The purified ce-MoS_2 dispersion was finally resuspended in Milli-Q water (18.2 MΩ cm) and scooped onto TEM grids for analysis.

STEM microscopy

Atomic-resolution STEM analysis was performed using a JEOL ARM-300F double-corrected microscope equipped with an ADF detector. The microscope operated at an acceleration voltage of 80 kV, and the convergence semi-angle was 22 mrad, the detector acceptance angles set at 54–220 mrad (inner-outer angles) to enhance atomic number contrast.

Results and discussion

Fig. 1 presents atomic-resolution STEM-ADF imaging of distinct structural phases in monolayer MoS_2. The thermodynamically stable 1H–MoS_2 phase (Fig. 1a) crystallizes in the $P6/mmc$ space group,[37] featuring trigonal prismatic coordination of molybdenum centers with six sulfur atoms. In contrast, the metastable 1T-MoS_2 phase (Fig. 1b) adopts $P\bar{3}m1$ symmetry[38] with octahedrally coordinated metal centers, exhibiting metallic characteristics due to nonbonding d-band filling.[39] Structural transformation from 2H to 1T involves concerted sliding of sulfur planes along the <2100> direction by $a/\sqrt{3}$ lattice vectors (where $a = 3.16$ Å), inducing symmetry-breaking electronic state reconstruction. The 1T′-MoS_2 phase (Fig. 1c) emerges as a Peierls-distorted derivative of the 1T-MoS_2, forming 2a × 1a superlattices through zigzag-type Mo–Mo dimerization ($P21/m$ space group[38]). The intrachain Mo–Mo distances in the same zigzag chain is 3.11 Å along the a-axis, and with interchain separations of 2.72 Å (interchain) and 3.71 Å (adjacent chains),

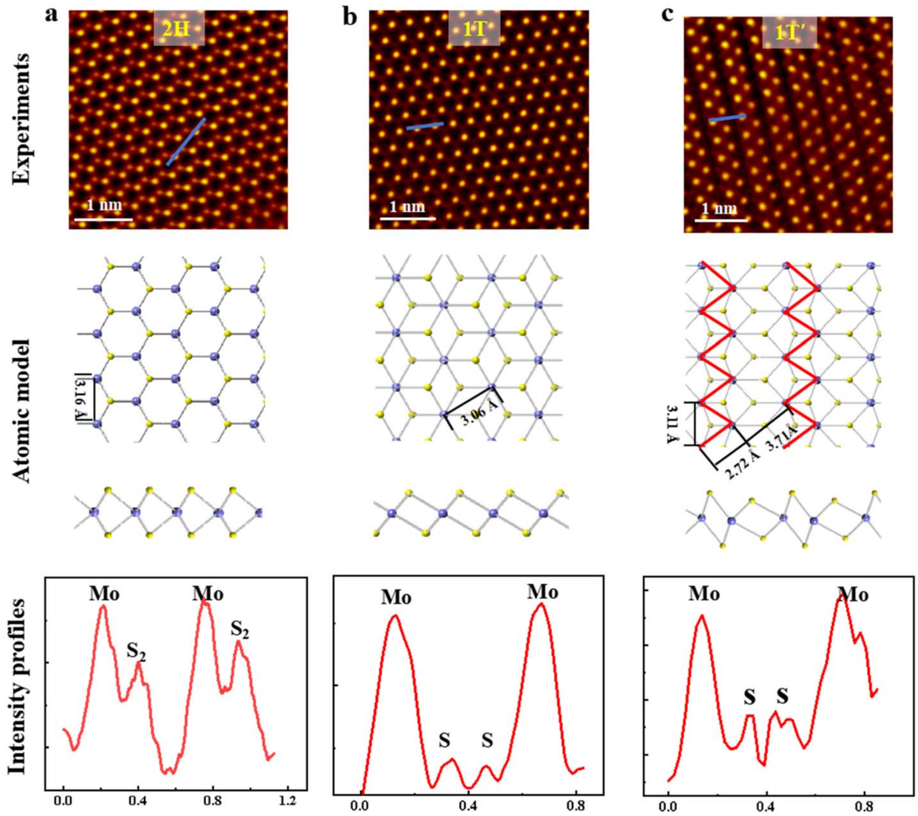

Fig. 1 Atomic-resolution STEM-ADF images of the monolayer MoS_2: (a) 2H; (b) 1T; (c) 1T′. Corresponding atomic structures are shown in the lower panels. The intensity line profiles of each STEM-ADF from the blue lines are depicted below. Mo, blue; S, yellow.

consistent with prior reports.[26] Crucially, this structural distortion induces deviation from planarity through atomic displacement vectors,[8] coupled with d-band splitting that governs its unique electronic properties. The distinct structural phases of monolayer MoS_2 can be identified through the atomic column intensity profile of STEM-ADF images. In the 1H–MoS_2, the signal of sulfur column enhancement arises from atomic overlap along the [0001] zone axis (Fig. 1a), yielding comparable Mo/S signal intensities.[40] Conversely, the 1T/1T′-MoS_2 monolayer exhibits sulfur intensity suppression due to in-plane delocalization (Fig. 1b and c), producing characteristic hexagonal patterns with Mo-dominated contrast. These distinct imaging signatures – honeycomb *vs.* hexagonal lattice symmetries with differential Mo/S intensity ratios – provide definitive phase identification criteria for monolayer MoS_2 system.

Electron diffraction analysis serves as a critical phase identification tool through characteristic symmetry features. Fig. S1† displays simulated electron diffraction patterns (EDP) along the [0001] zone axis for 2H, 1T, and 1T′-MoS_2. The 1H–MoS_2 exhibits sixfold rotational symmetry in its EDP (Fig. S1a†), while the 1T-MoS_2 maintains similar symmetry but with a 3% lattice contraction[41] (Fig. S1b†). The 1T′-MoS_2 is unambiguously identified by superstructure reflections at 1/2(10–10) and (01–10) positions (highlighted in green/yellow circles, Fig. S1c†), confirming the 2a × 1a basal plane periodicity. These satellite spots, arising from Peierls-type structural modulation, reveal the distinctive symmetry of the 1T′-MoS_2.

The X-ray diffraction (XRD) pattern and Raman spectra of 2H and 1T′-MoS_2 are shown in Fig. S2,† indicating that the synthesized ce-MoS_2 was mainly of 1T′ phase. Low-magnification STEM-ADF imaging (Fig. S3a†) confirms the monolayer continuity of ce-MoS_2 on the scale of hundreds of nanometers. The corresponding selected-area electron diffraction (SAED) pattern (Fig. S3b†) demonstrates predominant 1T′ phase characteristics through 5.6 $Å^{-1}$ superlattice reflections (green circles), consistent with the 2a × 1a reconstruction. Atomic-resolution imaging (Fig. S3c†) resolves one-dimensional zigzag Mo–Mo chains with characteristic intrachain distances of 2.8 Å and interchain separations of 3.7 Å, quantitatively matching the 2 × 1 superstructure parameters of 1T′-MoS_2. Fast Fourier transform (FFT) analysis of the STEM image (inset, Fig. S3c†) corroborates this structural interpretation, exhibiting directional superlattice spots (green arrow) aligned with the [0001] zone axis. The phase stability hierarchy is rationalized through first-principles calculations,[16] revealing lithium concentration-dependent energetics. At Li intercalation levels >20%, octahedrally coordinated phases gain thermodynamic preference. But 1T phase is the most unstable and has a high distortion tendency, the dimerization along one direction reduces the total energy by 0.3 eV per Mo compared to the undistorted 1T structure. This distortion-driven stabilization mechanism explains the predominance of 1T′ phase observed in ce-MoS_2, as evidenced by our combined STEM images and diffraction analyses.

Structural characterization reveals that the ce-MoS_2 exhibits a polymorphic composition comprising three distinct phases: the semiconducting 1H–MoS_2 (Fig. 1a), metastable 1T-MoS_2 (Fig. 1b), and predominant 1T′-MoS_2 (Fig. 1c). Quantitative analysis shows significantly lower phase fractions of 2H–MoS_2 and 1T-MoS_2 compared to 1T′-MoS_2, consistent with prior reports.[42] Notably, we identified a unique coexistence of 2H and 1T domains through atomic-resolution imaging (Fig. 2a), demonstrating the formation of coherent heterostructures interfaces within individual monolayer. FFT analysis confirms the single-crystalline nature of these heterostructures, evidenced by shared diffraction patterns between adjacent phases (inset, Fig. 2a). A remarkable interfacial feature emerges at the 2H/1T′ boundary, exhibiting atomically abrupt transition along the zigzag crystallographic direction (Fig. 2d). This sharp grain boundary – crucial for efficient carrier separation in optoelectronic applications – preserves the hexagonal Mo sublattice without detectable dislocations or lattice distortion, as confirmed by continuous atomic arrangement and single-set hexagonal FFT spots. Line profile analysis across the interface (Fig. 2e) reveals a discontinuous sulfur sublattice: the 2H region maintains alternating S–Mo coordination while the 1T′ side shows exclusive Mo periodicity, confirming chemically distinct yet structurally coherent grain boundaries. Complementary geometric phase analysis (GPA) (Fig. S3†) indicates minimal strain accumulation (<0.5%) near the interface despite non-ideal Mo coordination at boundary sites. The coexistence of 1T′ and 2H phases in monolayer MoS_2 creates atomically sharp grain boundaries with distinct electronic and structural properties. Thesegrain boundaries are characterized by abrupt transitions in coordination geometry—1T′ phase exhibits octahedral Mo coordination, while 2H phase maintains trigonal prismatic coordination—resulting in a unique localized charge redistribution. Recent density functional theory (DFT) studies[43] reveal that the 1T′/2H boundary exhibits a sub-nanometer width, with minimal atomic reconstruction, preserving the intrinsic electronic properties of both phases. The interfacial dipole, arising from charge transfer between phases, introduces a built-in electric field that can modulate carrier transport and catalytic activity. Furthermore, the sharpness of this interface enables precise control over phase heterostructures, offering opportunities for designing novel electronic devices and tunable catalysts.

Unlike the structurally stable 2H–MoS_2 under imaging conditions, the 1T′-MoS_2 demonstrated beam-sensitive structural dynamics during STEM observation. Fig. 3a–d show that the arrays of zigzag chains with original orientation was sequentially reorganized under electron beam irradiation to form the three-oriented shorter chain clusters. This ordered configurational evolution contrasts starkly with stochastic defect generation, suggesting a correlated atomic rearrangement mechanism. Atomic-scale tracking of the transformation process reveals that reorientation initiates *via* tetramer cluster kinking (Fig. 3g). Bond-length analysis provides critical differentiation between structural motifs: diamond clusters exhibit alternating Mo–Mo distances of 0.34 nm and 0.29 nm along the [−12−10] direction (Fig. 3e and f), distinct from the uniform 0.31 nm spacing in pristine zigzag chains. These metrics confirm that reorientation arises from coordinated downward displacements of Mo atoms (labeled A–D in Fig. 3g), involving sequential metal–metal bond cleavage and reformation. The resultant chain reorientations occurred at characteristic 120° or 60° angles (Fig. 3d), directly reflecting the threefold symmetry of the 1T′ phase and its three equivalent crystallographic directions. Concomitant FFT analysis reveals degeneracy of 1T′ superstructure spots, evolving from unidirectional ordering to a triply degenerate superposition pattern (highlighted by color-coded arrows in Fig. 3h). This symmetry-constrained anisotropic restructuring suggests potential for in-plane electronic anisotropy, as evidenced by prior reports of direction-dependent conductivity in such systems.[44] The observed electron beam-induced orientational switching in 1T′-MoS_2 not only

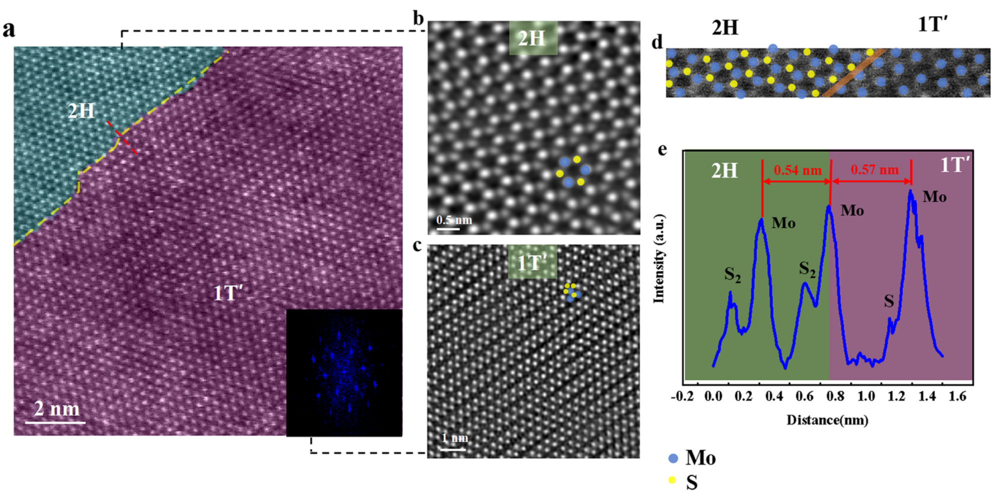

Fig. 2 (a) STEM-ADF image of an atomically thin phase boundary (indicated by the yellow dashed line) between the 2H and 1T′ phase in a monolayer ce-MoS_2. (b) STEM-ADF image of 2H phase of ce-MoS_2. (c) STEM-ADF image of 1T′ phase of ce-MoS_2. (d) The enlarged STEM-ADF image at the 1T′/2H grain boundary. (e) Intensity line profile of the red dashed line in (a) confirming the 1T′/2H phase boundary.

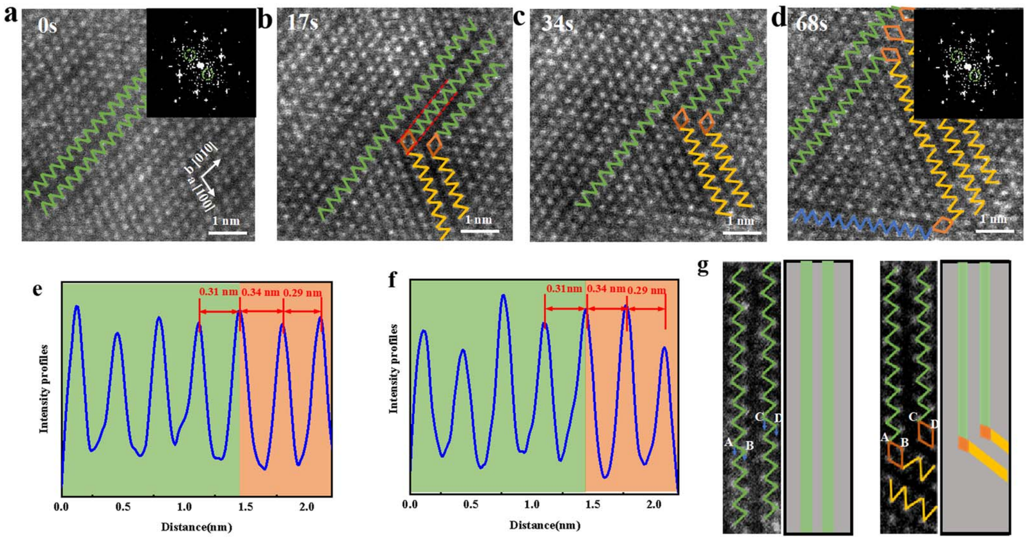

Fig. 3 (a–d) Series of STEM-ADF images showing the evolution of 1T′ phase as a function of time under electron beam irradiation. The inset is the corresponding FFT pattern. (e and f) The intensity line profiles of each STEM-ADF from the red lines in (b). (g) The sequential ADF image of 1T′ phase of changing the orientation diamond chains, scale bar 0.5 nm. The schemes on the right side represent the conduction channel before (green) and after (yellow) electron beam modulation.

unveils metastable phase dynamics but also highlights opportunities for engineering anisotropic charge transport pathways in 2D materials through controlled symmetry breaking. One of the direct consequences of electron beam-induced zigzag chain orientation switching in 1T′-MoS_2 monolayer is the formation of coherent twin boundaries between zigzag chains between different orientations. Unlike their three-dimensional counterparts, in which the regional boundary is 2D, the boundaries formed between the domains of 2D-MX_2 monolayer are quasi-1D, which may give them unique properties and provide a rich platform for boundary engineering. Moreover, 1T′-MoS_2 will inevitably reduce the domain size due to the existence of domain boundaries, which can improve the phase and charge uniformity in the electrochemical phase transition process. This phase reconstruction can be used to improve the energy storage performance of MoS_2 batteries.

Recent calculations[16,32] confirm that the 1T′-MoS_2 represents the most thermodynamically stable octahedral polymorph of MoS_2. Unlike the 2H → 1T phase transition involving global structural reorganization, the orientation switching of zigzag chains in 1T′-MoS_2 occurs through localized distortions of the Mo–S octahedral coordination geometry. Therefore, the energy require for this process is minimal. First-principles calculations[45] quantify this process with an exceptionally low energy barrier of <0.15 eV per formula unit – a value far below conventional phase transition thresholds. Such ultralow activation energies render the system highly susceptible to external stimuli, explaining the observed electron beam-induced reorientation phenomena. The underlying mechanism involves energy transfer from incident electrons through high angle elastic scattering events. These interactions impart sufficient kinetic energy to lattice atoms (estimated to exceed the aforementioned energy barrier) to initiate coordinated Mo displacements. Crucially, the reorientation process preserves the octahedral framework while reconfiguring metal–metal bonding patterns, enabling dynamic switching between degenerate zigzag chain orientations. This metastability highlights the unique potential of 1T′-MoS_2 for designing stimuli-responsive nanomaterials with field-tunable anisotropic properties. The observed transformation dynamics reveal that tetramer clusters act as transient intermediates during the zigzag chain reorientation process in monolayer 1T′-MoS_2 (Fig. 3g). Previous theoretical studies suggest that charge stabilization is critical for diamond cluster formation,[16] a condition potentially met in our system through surface ionization or direct electron beam charging during STEM imaging. The ephemeral nature of these clusters implies insufficient sustained charge stabilization under experimental conditions, consistent with the absence of prolonged tetramer stability in our samples. Quantitative analysis of interfacial energetics provides further mechanistic insights: density functional theory (DFT) calculations estimate the twin boundary formation energy in 1T′-MoS_2 at ∼27 meV $Å^{-1}$,[45] orders of magnitude lower than the dislocation core energy (∼hundreds of meV $Å^{-1}$).[45] This stark contrast in energy scales rationalizes the preferential formation of orientation variants over dislocation-mediated structural degradation, enabling facile interconversion between degenerate zigzag configurations. Additional evidence supporting the 1T′ phase's configurational flexibility is presented in Fig. S7,† demonstrating analogous symmetry-governed restructuring pathways.

Theoretical investigations[31] reveal that the 1T′-MoS_2 phase is metastable under ambient conditions, with a calculated minimum energy barrier of 0.78 eV for the 1T′ → 2H transition. This thermodynamic landscape suggests that 1T′-MoS_2 can persist indefinitely under appropriate chemical or thermal

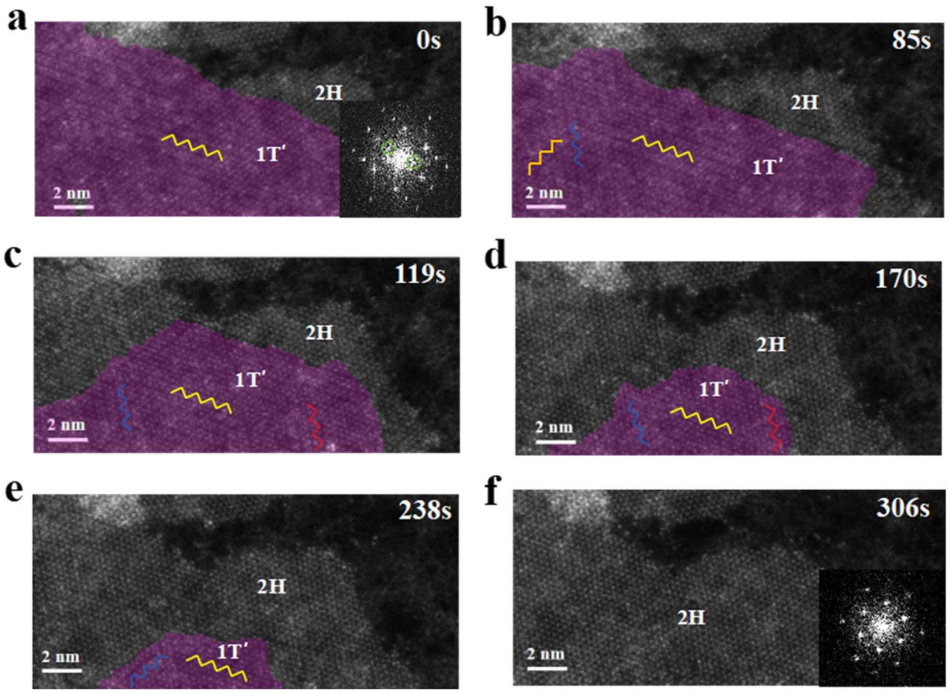

Fig. 4 1T′ → 2H phase transition in monolayer MoS_2. (a–f) Series of STEM-ADF images showing the 1T′ → 2H phase transition as a function of time under electron beam irradiation. The insets are the corresponding FFT pattern.

stabilization – a prediction experimentally validated in our work. As shown in Fig. S8,† ce-MoS_2 retains its 1T′ configuration even after two days of air exposure, confirming its remarkable environmental stability. To probe 1T′ to 2H phase transition dynamics, we systematically monitored electron beam-induced structural evolution (Fig. 4). It is found that the 1T′-MoS_2 first changed orientation of zigzag chains and transformed into shorter chains with three orientations (Fig. 4b). As the time of the electron beam irradiation increased, the area of the 1T′ phase gradually decreased, and the 1T′ phase gradually relaxed to 2H phase (Fig. 4c–e), and finally the entire MoS_2 was transformed to 2H phase (Fig. 4f). This sequential transformation confirms the metastable nature of 1T′-MoS_2, where energy inputs exceeding the activation barrier drive structural relaxation to the thermodynamically favored 2H phase. The disappearance of 1T′ superstructure spots in FFT patterns (insets, Fig. 4a and f) provides further evidence of this irreversible phase transition. These results confirm that the 1T′ phase is energetically preferred metastable phase, and when the input energy exceeds the metastable barrier energy, the 1T′ phase will relax back to 2H. Complementary experiments (Fig. S9†) demonstrate the universality of this beam-driven transformation mechanism. We propose that prolonged electron irradiation enables cumulative energy transfer through inelastic scattering events, inducing sulfur sublattice displacements that destabilize the 1T′ configuration. These atomic-scale rearrangements ultimately restore the trigonal prismatic coordination characteristic of the 2H phase. Notably, the observed partial transitions (Fig. 4c–e) likely arise from localized energy fluctuations during characterization, highlighting the delicate energy balance governing phase stability.

Conclusion

In this study, we present a comprehensive investigation of structural evolution in monolayer 1T′-MoS_2 through atomic-scale structural analysis. We systematically characterized the crystallographic configurations and corresponding diffraction signatures of distinct polytypes by using AC-STEM. Of particular interest, real-time STEM imaging captured dynamic structural reorganization in the metastable 1T′ phase under electron beam irradiation. The transformation mechanism involves progressive reconfiguration of metal–metal bonding networks, manifested as the emergence of diamond-shaped coordination clusters and subsequent development of novel crystallographic orientations. Controlled electron beam exposure was demonstrated to induce complete 1T′-to-2H phase transition. Crucially, our atomic-resolution imaging unveiled atomically sharp 2H/1T′ interfacial domain boundary with coherent lattice matching. Such defect-free heterophase boundaries exhibit exceptional interfacial continuity, a critical feature for designing 2D heterostructure devices requiring abrupt electronic property modulation. These findings provide new insights into the kinetic pathways of structural transformations in layered chalcogenides. This work establishes a framework for understanding metastable phase dynamics in low-dimensional systems while advancing methodologies for precision nanoscale phase patterning.

Data availability

The data that support the findings of this study are available from the corresponding author upon reasonable request.

Author's contributions

L. Xu developed the work and performed the experiment. F. Li and J. Qi guided and analyzed the work. L. Xu wrote the manuscript. All authors participated in the manuscript review.

Conflicts of interest

The authors declare no conflict of interest.

Acknowledgements

This work was supported by Beijing Natural Science Foundation (2254090), the National Key R&D Program of China (2024YFA1208201) and the Guangdong Basic and Applied Basic Research Foundation (2023A1515011209).

References

1 B. Radisavljevic, A. Radenovic, J. Brivio, V. Giacometti and A. Kis, Single-layer MoS_2 transistors, *Nat. Nanotechnol.*, 2011, **6**(3), 147–150.
2 T. Cao, G. Wang, W. Han, H. Ye, C. Zhu, J. Shi, Q. Niu, P. Tan, E. Wang, B. Liu and J. Feng, Valley-selective circular dichroism of monolayer molybdenum disulphide, *Nat. Commun.*, 2012, **3**(1), 887.
3 K. F. Mak, K. He, J. Shan and T. F. Heinz, Control of valley polarization in monolayer MoS_2 by optical helicity, *Nat. Nanotechnol.*, 2012, **7**(8), 494–498.
4 A. Splendiani, L. Sun, Y. Zhang, T. Li, J. Kim, C.-Y. Chim, G. Galli and F. Wang, Emerging Photoluminescence in Monolayer MoS2, *Nano Lett.*, 2010, **10**(4), 1271–1275.
5 K. F. Mak, C. Lee, J. Hone, J. Shan and T. F. Heinz, Atomically Thin MoS_2: A New Direct-Gap Semiconductor, *Phys. Rev. Lett.*, 2010, **105**(13), 136805.
6 F. Jaramillo Thomas, P. Jørgensen Kristina, J. Bonde, H. Nielsen Jane, S. Horch and I. Chorkendorff, Identification of Active Edge Sites for Electrochemical H_2 Evolution from MoS_2 Nanocatalysts, *Science*, 2007, **317**(5834), 100–102.
7 J. Kibsgaard, Z. Chen, B. N. Reinecke and T. F. Jaramillo, Engineering the surface structure of MoS_2 to preferentially expose active edge sites for electrocatalysis, *Nat. Mater.*, 2012, **11**(11), 963–969.
8 M. Chhowalla, H. S. Shin, G. Eda, L.-J. Li, K. P. Loh and H. Zhang, The chemistry of two-dimensional layered transition metal dichalcogenide nanosheets, *Nat. Chem.*, 2013, **5**(4), 263–275.
9 D. Voiry, A. Mohite and M. Chhowalla, Phase engineering of transition metal dichalcogenides, *Chem. Soc. Rev.*, 2015, **44**(9), 2702–2712.
10 Y. Xiao, M. Zhou, J. Liu, J. Xu and L. Fu, Phase engineering of two-dimensional transition metal dichalcogenides, *Sci. China Mater.*, 2019, **62**(6), 759–775.
11 L. F. Mattheiss, Band Structures of Transition-Metal-Dichalcogenide Layer Compounds, *Phys. Rev. B*, 1973, **8**(8), 3719–3740.
12 C. S. Tang, X. Yin and A. T. S. Wee, 1D chain structure in 1T′-phase 2D transition metal dichalcogenides and their anisotropic electronic structures, *Applied Physics Reviews*, 2021, **8**(1), 011313.
13 I. Tyulnev, Á. Jiménez-Galán, J. Poborska, L. Vamos, P. S. J. Russell, F. Tani, O. Smirnova, M. Ivanov, R. E. F. Silva and J. Biegert, Valleytronics in bulk MoS_2 with a topologic optical field, *Nature*, 2024, **628**(8009), 746–751.
14 C. Jiang, A. Rasmita, H. Ma, Q. Tan, Z. Zhang, Z. Huang, S. Lai, N. Wang, S. Liu, X. Liu, T. Yu, Q. Xiong and W.-b. Gao, A room-temperature gate-tunable bipolar valley Hall effect in molybdenum disulfide/tungsten diselenide heterostructures, *Nat. Electron.*, 2022, **5**(1), 23–27.
15 H. L. Zhuang, M. D. Johannes, A. K. Singh and R. G. Hennig, Doping-controlled phase transitions in single-layer MoS_2, *Phys. Rev. B*, 2017, **96**(16), 165305.
16 M. Kan, J. Y. Wang, X. W. Li, S. H. Zhang, Y. W. Li, Y. Kawazoe, Q. Sun and P. Jena, Structures and Phase Transition of a MoS_2 Monolayer, *J. Phys. Chem. C*, 2014, **118**(3), 1515–1522.
17 X. Qian, J. Liu, L. Fu and J. Li, Quantum spin Hall effect in two-dimensional transition metal dichalcogenides, *Science*, 2014, **346**(6215), 1344.
18 R. Zhang, I. L. Tsai, J. Chapman, E. Khestanova, J. Waters and I. V. Grigorieva, Superconductivity in Potassium-Doped Metallic Polymorphs of MoS_2, *Nano Lett.*, 2016, **16**(1), 629–636.
19 Y. Sun, S. C. Wu, M. N. Ali, C. Felser and B. Yan, Prediction of Weyl semimetal in orthorhombic $MoTe_2$, *Phys. Rev. B*, 2015, **92**(16), 161107.
20 Y. Qi, P. G. Naumov, M. N. Ali, C. R. Rajamathi, W. Schnelle, O. Barkalov, M. Hanfland, S.-C. Wu, C. Shekhar, Y. Sun, V. Süß, M. Schmidt, U. Schwarz, E. Pippel, P. Werner, R. Hillebrand, T. Förster, E. Kampert, S. Parkin, R. J. Cava, C. Felser, B. Yan and S. A. Medvedev, Superconductivity in Weyl semimetal candidate $MoTe_2$, *Nat. Commun.*, 2016, **7**(1), 11038.
21 X. Chen, Z. Chen and J. Li, Critical electronic structures controlling phase transitions induced by lithium ion intercalation in molybdenum disulphide, *Chin. Sci. Bull.*, 2013, **58**(14), 1632–1641.
22 S. N. Shirodkar and U. V. Waghmare, Emergence of Ferroelectricity at a Metal-Semiconductor Transition in a 1T Monolayer of MoS_2, *Phys. Rev. Lett.*, 2014, **112**(15), 157601.
23 M. H. Whangbo and E. Canadell, Analogies between the concepts of molecular chemistry and solid-state physics concerning structural instabilities. Electronic origin of the structural modulations in layered transition metal dichalcogenides, *J. Am. Chem. Soc.*, 1992, **114**(24), 9587–9600.
24 M. Kertesz and R. Hoffmann, Octahedral *vs.* trigonal-prismatic coordination and clustering in transition-metal dichalcogenides, *J. Am. Chem. Soc.*, 1984, **106**(12), 3453–3460.

25 R. Peierls, Zur Theorie der elektrischen und thermischen Leitfähigkeit von Metallen, *Ann. Phys.*, 1930, **396**(2), 121–148.

26 M. Calandra, Chemically exfoliated single-layer MoS_2: Stability, lattice dynamics, and catalytic adsorption from first principles, *Phys. Rev. B*, 2013, **88**(24), 245428.

27 T. A. J. Loh and D. H. C. Chua, Origin of Hybrid 1T- and 2H-WS_2 Ultrathin Layers by Pulsed Laser Deposition, *J. Phys. Chem. C*, 2015, **119**(49), 27496–27504.

28 Y. C. Lin, D. O. Dumcenco, Y. S. Huang and K. Suenaga, Atomic mechanism of the semiconducting-to-metallic phase transition in single-layered MoS_2, *Nat. Nanotechnol.*, 2014, **9**(5), 391–396.

29 K. He, C. Poole, K. F. Mak and J. Shan, Experimental Demonstration of Continuous Electronic Structure Tuning *via* Strain in Atomically Thin MoS_2, *Nano Lett.*, 2013, **13**(6), 2931–2936.

30 H. Guo, N. Lu, L. Wang, X. Wu and X. C. Zeng, Tuning Electronic and Magnetic Properties of Early Transition-Metal Dichalcogenides *via* Tensile Strain, *J. Phys. Chem. C*, 2014, **118**(13), 7242–7249.

31 S. S. Chou, N. Sai, P. Lu, E. N. Coker, S. Liu, K. Artyushkova, T. S. Luk, B. Kaehr and C. J. Brinker, Understanding catalysis in a multiphasic two-dimensional transition metal dichalcogenide, *Nat. Commun.*, 2015, **6**, 8311.

32 X. L. Fan, Y. Yang, P. Xiao and W.-M. Lau, Site-specific catalytic activity in exfoliated MoS_2 single-layer polytypes for hydrogen evolution: basal plane and edges, *J. Mater. Chem. A*, 2014, **2**(48), 20545–20551.

33 D. Voiry, M. Salehi, R. Silva, T. Fujita, M. Chen, T. Asefa, V. B. Shenoy, G. Eda and M. Chhowalla, Conducting MoS_2 Nanosheets as Catalysts for Hydrogen Evolution Reaction, *Nano Lett.*, 2013, **13**(12), 6222–6227.

34 D. Merki and X. Hu, Recent developments of molybdenum and tungsten sulfides as hydrogen evolution catalysts, *Energy Environ. Sci.*, 2011, **4**(10), 3878–3888.

35 J. N. Coleman, M. Lotya, A. O'Neill, S. D. Bergin, P. J. King, U. Khan, K. Young, A. Gaucher, S. De, R. J. Smith, I. V. Shvets, S. K. Arora, G. Stanton, H.-Y. Kim, K. Lee, G. T. Kim, G. S. Duesberg, T. Hallam, J. J. Boland, J. J. Wang, J. F. Donegan, J. C. Grunlan, G. Moriarty, A. Shmeliov, R. J. Nicholls, J. M. Perkins, E. M. Grieveson, K. Theuwissen, D. W. McComb, P. D. Nellist and V. Nicolosi, Two-Dimensional Nanosheets Produced by Liquid Exfoliation of Layered Materials, *Science*, 2011, **331**(6017), 568.

36 A. Yan, C. S. Ong, D. Y. Qiu, C. Ophus, J. Ciston, C. Merino, S. G. Louie and A. Zettl, Dynamics of Symmetry-Breaking Stacking Boundaries in Bilayer MoS_2, *J. Phys. Chem. C*, 2017, **121**, 22559–22566.

37 E. Benavente, M. A. Santa Ana, F. Mendizábal and G. González, Intercalation chemistry of molybdenum disulfide, *Coord. Chem. Rev.*, 2002, **224**(1), 87–109.

38 A. T. Hoang, S. M. Shinde, A. K. Katiyar, K. P. Dhakal, X. Chen, H. Kim, S. W. Lee, Z. Lee and J.-H. Ahn, Orientation-dependent optical characterization of atomically thin transition metal ditellurides, *Nanoscale*, 2018, **10**(46), 21978–21984.

39 R. Kappera, D. Voiry, S. E. Yalcin, B. Branch, G. Gupta, A. D. Mohite and M. Chhowalla, Phase-engineered low-resistance contacts for ultrathin MoS_2 transistors, *Nat. Mater.*, 2014, **13**(12), 1128–1134.

40 X.-L. Fan, Y. Yang, P. Xiao and W.-M. Lau, Site-specific catalytic activity in exfoliated MoS_2 single-layer polytypes for hydrogen evolution: basal plane and edges, *J. Mater. Chem. A*, 2014, **2**(48), 20545–20551.

41 S. Chen, L. Wang, R. Shao, J. Zou, R. Cai, J. Lin, C. Zhu, J. Zhang, F. Xu, J. Cao, J. Feng, J. Qi and P. Gao, Atomic structure and migration dynamics of MoS_2/Li_xMoS_2 interface, *Nano Energy*, 2018, **48**, 560–568.

42 G. Eda, T. Fujita, H. Yamaguchi, D. Voiry, M. Chen and M. Chhowalla, Coherent Atomic and Electronic Heterostructures of Single-Layer MoS-$_2$, *ACS Nano*, 2012, **6**(8), 7311–7317.

43 B. Liu, J. Xiong, S. Xu, X. Luo, W. Yao, S. Liu, Y. Du, Q. Zhang, Y. Gao and B. Wang, Unveiling the superior hydrogen evolution reaction activity of 1T-2H MoS_2 heterointerface by on-chip microdevices, *Nano Res.*, 2025, **18**(1), 94907020.

44 Y.-C. Lin, H.-P. Komsa, C.-H. Yeh, T. Björkman, Z.-Y. Liang, C.-H. Ho, Y.-S. Huang, P.-W. Chiu, A. V. Krasheninnikov and K. Suenaga, Single-Layer ReS_2: Two-Dimensional Semiconductor with Tunable In-Plane Anisotropy, *ACS Nano*, 2015, **9**(11), 11249–11257.

45 W. Li and J. Li, Ferroelasticity and domain physics in two-dimensional transition metal dichalcogenide monolayers, *Nat. Commun.*, 2016, **7**(1), 10843.